Eur. Phys. J. C (2024) 84:1187
https://doi.org/10.1140/epjc/s10052-024-13561-4

THE EUROPEAN PHYSICAL JOURNAL C

Regular Article

Theoretical Physics

Imprints of the Einasto density profile and complexity factor on traversable wormholes in $f(R, T)$ theory

Tayyab Naseer[1,2,a], **M. Sharif**[1,b], **Mona Faiza**[1,c], **Baiju Dayanandan**[3,d]

[1] Department of Mathematics and Statistics, The University of Lahore, 1-KM Defence Road, Lahore 54000, Pakistan
[2] Research Center of Astrophysics and Cosmology, Khazar University, 41 Mehseti Street, AZ1096 Baku, Azerbaijan
[3] Natural and Medical Sciences Research Centre, University of Nizwa, Nizwa, Oman

Received: 30 September 2024 / Accepted: 29 October 2024

Abstract The focus of this work is centered on determining whether traversable wormholes admitting Einasto density profile exist within the framework of $f(R, T)$ gravity. Using the Morris–Thorne spacetime, we express the wormhole configuration and formulate the anisotropic gravitational equations for a particular linear modified model. Afterwards, by considering two different (constant and variable) redshift functions, we derive the shape function for wormholes and examine its potential stability. The developed functions conform to the necessary conditions and form a connection between two spacetime regions that are asymptotically flat. We also examine the viability of resulting wormhole solutions by verifying their violation with the null energy conditions. We also investigate the active gravitational mass and the complexity factor for our solutions. The later quantity is found to be negative near the wormhole throat and becomes zero when moving away from this point. Further, various methods of stability analysis are utilized to assess the developed models. Our results suggest that the constructed wormhole geometries meet the necessary conditions, thereby existing within the considered modified gravity.

1 Introduction

Recent discoveries about the cosmic rapid expansion have driven theoretical physicists to study and decode the mechanisms behind this extraordinary dynamic phenomenon [1,2]. This accelerated expansion has been revealed through observations like those of supernova Ia and others, contradicting previous expectations of a decelerating universe [3–5]. Scientists claimed that the rapid expansion is caused by dark energy because of its powerful repulsive force. Numerous theoretical and hypothetical models have been suggested and reviewed to understand this prodigy. In cosmology, the Λ-CDM model is a key framework for elucidating the characteristics of dark energy. Through this model, one can understand how dark energy influences the geometric structure of the universe. This model has made significant progresses in dealing with various issues, yet it continues to face problems related to the fine-tuning and cosmic coincidence. The challenge of dealing with these problems highlights the need for a deeper insight into gravity, potentially offering new ways to address existing inconsistencies.

The $f(R)$ theory was initially introduced by Buchdahl in 1970 [6], who altered the action of the general theory of relativity (GR) by substituting the Ricci scalar R with its generic function. Researchers employed this framework to study the attributes of various celestial objects [7–11]. By employing the $f(R)$ gravity models, a novel perspective on cosmic structure and gravitational interactions has been emerged, potentially contrasting with GR's predictions. Bamba et al. [12] examined the $\Lambda - CDM$ like universe in the light of various models and also investigated some properties of dark energy. Nojiri and Odintsov [13] confirmed the stability of $f(R)$ theory through various models which are consistent with the solar system data to examine unexplained phenomena in the cosmos. Recently, Agrawal et al. [14] studied a particular cosmological model within this gravity theory by taking into account an isotropic perfect fluid distribution along with different forms of the curvature scalar and addressed the concept of gravitational baryogenesis. This theory has been modified by Bertolami et al. [15] to include the effect

[a] e-mail: tayyabnaseer48@yahoo.com; tayyab.naseer@math.uol.edu.pk (corresponding author)
[b] e-mail: msharif.math@pu.edu.pk (corresponding author)
[c] e-mail: monafaiza.math@gmail.com
[d] e-mail: baiju@unizwa.edu.om

Published online: 20 November 2024

of matter-geometry coupling, named the $f(R, L_m)$ theory. They added the the matter Lagrangian into the functional $f(R)$ whose impact on certain exotic geometries have been studied [16].

Another extension of the $f(R)$ framework was introduced by Harko et al. [17], which included the trace of the energy-momentum tensor (T) and resulted in the development of $f(R, T)$ gravity. They utilized the metric formalism to establish the corresponding field equations. Due to the presence of T, this theory is observed to lack conservation, introducing an additional force (linked to matter parameters like density and pressure [18]) that hampers the geodesic trajectories of test particles in the gravitational field. Singh and Kumar [19] used the the minimal model of the form $R + 2\beta T$ with bulk viscosity to discuss the impact of the second term on cosmic expansion for various positive and negative choices of β. This theory, as explored by Sharif and Zubair [20], has the potential to reproduce various cosmological phenomena, including both phantom and non-phantom regimes and Λ cold dark matter. Baffou et al. [21] conducted a comprehensive analysis with the help of two different modified models and discussed them in the cosmological background. They have done this for both low and high redshift ranges and found their results to be compatible with observational data. Tretyakov [22] examined this theory with higher derivatives of the matter field and explored stability criteria to address fundamental issues like ghosts and tachyons. A comprehensive review of different astrophysical and cosmological phenomena within this gravity has been done in [23–30]. Naseer and Sharif [31–35] have also determined multiple acceptable results in this context.

Current research is concentrating on both the theoretical and observational explorations of wormhole (WH) structures. Within the field of topology, WHs serve as connections between two spacetimes, which may be in the same universe or in separate universes, via a minimal surface called the throat. Similar to a metro network within a city that connects various locations, a WH serves to link different regions across the cosmos. One of the most remarkable characteristics of a WH is its ability to allow traveling in both directions, as long as the throat remains open. Understanding that traveling through WH might provide a shortcut within the spacetime is crucial. The different WH structures include: (i) an intra-universe, connecting two separate locations within one universe, and (ii) an inter-universe that links diverse areas across multiple universes. This idea suggests the existence of numerous universes, each with distinct properties and physical laws, potentially linked together by a WH. The term static is used for a WH whose throat radius remains unchanged and does not vary with time. The main difference between a dynamic WH and a static one is that the former has a throat radius that changes, altering the throat's width and shape. Classifying these structures is important due to their possible utility in theoretical scenarios involving interstellar travel or communication, as envisioned by astrophysicists.

Wormholes were first conceptualized in the innovative work of Misner and Wheeler [36,37] and Wheeler [38,39], aiming to describe how electric charge could be facilitated by spanning force lines across different spatial asymptotes. The investigation into the theoretical structure was continued by Einstein and Rosen [40], who examined its diverse characteristics. They developed a model namely the Einstein–Rosen bridge which is a theoretical construct suggesting a route through the universe. Fuller and Wheeler [41] highlighted that this bridge displays instability. It was suggested by their findings that the bridge would collapse [42,43] shortly after its creation, hindering the traverse of photons. The interaction of strong gravitational fields and spacetime characteristics influences this effect. Unfortunately, the Schwarzschild WH does not possess this characteristic and remains inaccessible to photons [44]. Morris and his team proposed a method to maintain the stability of a WH. They suggested that utilizing a specific type of matter known as "exotic" having repulsive properties, could effectively counteract the intense gravitational forces and help prevent the collapse of the WH.

In 1988, Morris and Thorne [45] were the first to propose the theoretical model of static traversable WHs. According to their proposal, a traversable WH requires a central passage that is designed to reduce its dimensions. To evaluate WH stability, matching conditions are used to match the properties on both sides of the throat [46]. Spherically shaped WHs have been extensively studied, and their feasibility is dependent on having the exotic matter. It was discovered that the presence of phantom energy facilitates the construction of these structures [47,48]. In their analysis, Kavya et al. [49] studied WH models in the $f(R, L_m)$ framework with several different shape functions and confirmed that these models met all the required criteria. After testing various equations of state on these models, it was found that only some of them satisfy the flaring-out criterion [50]. Some other interesting works are [51–60].

Einasto [61] stated that for a model to accurately describe real-world galactic systems, it must adhere to specific criteria. The initial step involves selecting a descriptive function, with the density profile being a sensible choice as it provides the necessary information to derive the gravitational potential, cumulative mass profile, and surface mass density. For a model to be physically valid, it must meet several conditions. For instance, the density profile must be non-negative, finite, and should decrease smoothly towards zero at larger radii. Additionally, the descriptive functions must be continuous and free of jump discontinuities, and certain moments of the mass function, such as those defining the systems effective radius, total mass, and central gravitational potential, need to be finite. Einasto [61] introduced various effective families of descriptive functions, including the promi-

nent Einasto density profile (EDP). This function has been employed by Einasto [62] to model $M31$. The same model was later applied by him [63] to a number of surrounding galaxies, including $M87$, the Milky way, $M32$, and others. Utilizing the EDP formulation offers a practical approach for constructing solutions involving dark matter WHs. The exploration of WH structures through such proposals is gaining more interest to investigate their possible existence.

Analyzing the properties of traversable WHs within the $f(R,T)$ theory is the central objective of this paper. We specifically explore the EDP model that assists in developing a viable interaction between WHs and dark matter halos. The article is structured according to the following scheme. Section 2 highlights the key features of the modified $f(R,T)$ theory and formulates gravitational equations corresponding to a minimal modified model. The EDP is explored in detail in Sect. 3. We then use this model with two different redshift functions to study WH geometries and explore the violation of null energy conditions. Section 4 covers the influence of active gravitational mass, whereas Sect. 5 examines the complexity factor and how it behaves at the WH throat. The stability analysis of the resulting models for all specified choices is presented in Sect. 6. Finally, the last section provides a summary of our main results.

2 $f(R,T)$ gravitational theory

The $f(R,T)$ theory can be expressed by the following action

$$I=\int\sqrt{-g}\left[\frac{f(R,T)}{16\pi}+L_m\right]dx^4. \tag{1}$$

Here, g indicates the determinant of the metric tensor $g_{\eta\nu}$ and L_m denotes the matter Lagrangian density. Formulating the generalized field equations in this extended theory results in

$$G_{\eta\nu}=8\pi T^{(tot)}_{\eta\nu}, \tag{2}$$

with $G_{\eta\nu}$ being the Einstein tensor providing a detailed description of the self-gravitating spacetime geometry, and $T^{(tot)}_{\eta\nu}$ represents the fluid configuration inside that geometry. The later term is defined as follows

$$T^{(tot)}_{\eta\nu}=\frac{1}{f_R}(T_{\eta\nu})+T^{(c)}_{\eta\nu}. \tag{3}$$

The tensors $T_{\eta\nu}$ and $T^{(c)}_{\eta\nu}$ in the overhead equation are related to the conventional fluid configuration and modified correction terms, respectively. The first factor can be expressed as

$$T_{\eta\nu}=-\frac{2}{\sqrt{-g}}\left[\frac{\delta(\sqrt{-g}L_m)}{\delta g^{\eta\nu}}\right]\Longrightarrow T_{\eta\nu}=g_{\eta\nu}L_m-\frac{\partial L_m}{\partial g_{\eta\nu}}. \tag{4}$$

Furthermore, the last term in Eq.(3) is characterized by

$$T^{(c)}_{\eta\nu}=\frac{1}{8\pi f_R}\Bigg[f_T T_{\eta\nu}+\left\{\frac{1}{2}(f-Rf_R)-f_T L_m\right\}g_{\eta\nu}-(g_{\eta\nu}\Box-\nabla_\eta\nabla_\nu)f_R+2f_T g^{\upsilon\varpi}\frac{\partial^2 L_m}{\partial g^{\eta\nu}\partial g^{\upsilon\varpi}}\Bigg]. \tag{5}$$

The symbols f_R and f_T indicate the partial derivatives of $f=f(R,T)$ with respect to R and T, respectively. The D'Alembertian operator, as expressed in the above equation, is given by $\Box\equiv\frac{1}{\sqrt{-g}}\partial_\eta(\sqrt{-g}g^{\eta\nu}\partial_\nu)$ along with ∇_η being the covariant derivative. Joining together Eqs.(2)-(5), we find

$$G_{\eta\nu}=\frac{1}{f_R}\Bigg[(8\pi+f_T)T_{\eta\nu}-(g_{\eta\nu}\Box-\nabla_\eta\nabla_\nu)f_R+\frac{1}{2}g_{\eta\nu}(f-Rf_R)-f_T g_{\eta\nu}L_m+2f_T g^{\upsilon\varpi}\frac{\partial^2 L_m}{\partial g^{\eta\nu}\partial g^{\upsilon\varpi}}\Bigg]. \tag{6}$$

At this stage, taking into account the Morris–Thorne metric is essential as it characterizes the geometry of WHs. This is mathematically expressed by

$$ds^2=-e^{\sigma(r)}dt^2+\left(1-\frac{H(r)}{r}\right)^{-1}dr^2+r^2\left(d\theta^2+\sin\theta d\phi^2\right), \tag{7}$$

where a redshift function is represented by $\sigma(r)$. Also, $H(r)$ is the function that represents the geometry of the WH, refers to the shape function.

The existence of anisotropic fluid distributions in celestial objects is a major subject of interest among astrophysicists, as many observations have pointed out differences in principal pressures due to several influencing factors. Following this, we assume that the geometry of the WH model is filled by the anisotropic fluid, with the expression provided as

$$T_{\eta\nu}=(\rho+P_t)U_\eta U_\nu+(P_r-P_t)\chi_\eta\chi_\nu+P_t g_{\eta\nu}. \tag{8}$$

It is necessary to define several terms at this moment to understand the impact of different factors on the WH geometry. For instance, ρ indicates the energy density, P_t is the tangential pressure, and P_r refers to the radial pressure. Additionally, U_η represents the four-velocity, and χ_η being the four-vector.

A standard modified model is necessarily required to make the developed results more meaningful and effective to understand. The literature offers several matter-geometry coupled $f(R,T)$ models, both minimal and non-minimal, however, we choose the following to make our calculation easy. This is defined as

$$f(R,T)=f_1(R)+f_2(T)=R+2\beta T, \tag{9}$$

with β being a constant and $T=-\rho+P_r+2P_t$. It is important to mention that this particular selection can help resolving the issue of the cosmological constant. In recent works on running vacuum cosmology and scale-dependent

gravity, an effective constant has been proposed as a potential means to alleviate the cosmological constant problem [64–68]. The relationship between the constant Λ and the Hubble parameter is given by $\Lambda_{eff} \propto H^2$ [69]. Additionally, validity of the term $2\beta T$ could lead to novel insights and a deeper understanding of astrophysical structures [70,71]. Using this modified functional form, researchers have been able to successfully address different phenomena [72–77]. By using Eq. (6) along with the model (9), the following independent field equations are produced as

$$\tilde{\rho} \equiv 8\pi\rho + \beta\left(3\rho - \frac{P_r}{3} - \frac{2P_t}{3}\right) = \frac{H'(r)}{8\pi r^2}, \tag{10}$$

$$\tilde{P_r} \equiv 8\pi P_r - \beta\left(\rho - \frac{7P_r}{3} - \frac{2P_t}{3}\right) = \frac{r^2\sigma' - H\left(r\sigma' + 1\right)}{4\pi r^3}, \tag{11}$$

$$\begin{aligned}\tilde{P_t} &\equiv 8\pi P_t - \beta\left(\rho - \frac{P_r}{3} - \frac{8P_t}{3}\right)\\ &= \frac{1}{32\pi r^3}\big[r\big\{2r^2\sigma'' + r^2\sigma'^2 - r\sigma'\big(H' - 2\big)\\ &\quad - 2H'\big\} - H\big(2r^2\sigma'' + r^2\sigma'^2 + r\sigma' - 2\big)\big].\end{aligned} \tag{12}$$

Here, $' = \frac{\partial}{\partial r}$ and the terms along with β result from modifying the action function of GR. From the equations mentioned above, the explicit expressions for the matter variables can be calculated as

$$\begin{aligned}\rho &= \frac{1}{48(\beta+2\pi)(\beta+4\pi)r^2}\\ &\quad\times\big[2\beta r(r-H)\sigma'' + \beta\sigma'\big\{r\big(H'+4\big) - 3H\big\}\\ &\quad + \beta r(r-H)\sigma'^2 + 16(\beta+3\pi)H'\big],\end{aligned} \tag{13}$$

$$\begin{aligned}P_r &= \frac{1}{48(\beta+2\pi)(\beta+4\pi)r^3}\\ &\quad\times\big[H\big\{2\beta r^2\sigma'' + \sigma' r\big(\beta r\sigma' - 21\beta - 48\pi\big) - 24\\ &\quad\times(\beta+2\pi)\big\} - r\big\{2\beta r^2\sigma'' + r\sigma'\big(\beta H' - 20\beta - 48\pi\big)\\ &\quad + \beta r^2\sigma'^2 - 8\beta H'\big\}\big],\end{aligned} \tag{14}$$

$$\begin{aligned}P_t &= \frac{1}{48(\beta+2\pi)(\beta+4\pi)r^3}\\ &\quad\times\big[r\big\{2(5\beta+12\pi)r^2\sigma'' + r\sigma'\big(8(\beta+3\pi) + (5\beta\\ &\quad + 12\pi)b'\big) + (5\beta+12\pi)r^2\sigma'^2 - 4(\beta+6\pi)H'\big\}\\ &\quad - H\big\{r\big(2(5\beta+12\pi)r\sigma''\\ &\quad + (5\beta+12\pi)r\sigma'^2 + 3(\beta+4\pi)\sigma'\big) - 12(\beta+2\pi)\big\}\big].\end{aligned} \tag{15}$$

In the next section, we shall derive two different shape functions by taking into account the EDP model along with two distinct choices of the redshift parameter and examine their viability by verifying their consistency with the required criteria.

3 Einasto density profile

To improve our understanding of the cosmic mysteries, such as the dark matter halos enveloping galaxy clusters, a more in-depth study of their attributes is necessary. Research using cosmological simulations and some other methods shown that different dark matter halos or galaxy clusters can be accurately described by distinct density models with three key parameters [78–81]. The EDP model, a three-dimensional variant of the Sérsic model, is frequently employed to describe dark matter halos [82,83]. The model is employed to analyze both the central regions of spiral galaxies and the brightness of old cosmic structures [84]. This is defined by [85]

$$\gamma(r) \equiv -\frac{d\ln\rho(r)}{d\ln r} \propto r^{\frac{1}{n}}, \tag{16}$$

where the symbol n refers to the Einasto index which characterizes the particular shape of the EDP model. The following density profile is derived from the integration of the above equation as

$$\ln\left(\frac{\rho(r)}{\rho_s}\right) = -c_n\left\{\left(\frac{r}{r_s}\right)^{\frac{1}{n}} - 1\right\}. \tag{17}$$

The parameter r_s represents the sphere's radius that includes half of the total mass, while c_n governs r_s, $\rho_s = \rho_s(r)$, and $\rho_0 = \rho_s e^{c_n}$. The constant c_n ensures that ρ_s defines the radius surrounding half of the mass. It must be highlighted that multiple parameterizations of the EDP model have been proposed, each with its unique set of free parameters. In dark matter-halo realm, a widely used representation has the following form

$$\ln\left(\frac{\rho(r)}{\rho_{-2}}\right) = -2n\left\{\left(\frac{r}{r_s}\right)^{\frac{1}{n}} - 1\right\}, \tag{18}$$

when r_{-2} and ρ_{-2} represent the radius and density, respectively. Also, the quantity $\rho(r)$ follows a direct proportionality to r^{-2} and can be written as

$$\rho(r) = \rho_0 e^{-(\frac{r}{h})^{\frac{1}{n}}}, \tag{19}$$

with h and ρ_0 being the scale length and central density defined by

$$h = \frac{r_s}{c_n^n} = \frac{r_{-2}}{(2n)^n}, \quad \rho_0 = \rho_s e^{c_n} = \rho_{-2}e^{2n}. \tag{20}$$

For the model to accurately reflect real galactic formations, it must conform to certain standards, such as those related to mass profile, gravitational potential, and surface mass density [86]. Choosing the appropriate descriptive functions is the key to accurately modeling any galactic structure. Considering the fundamental role of the density profile in these functions, it becomes the most favorable option in this context. The term $\rho(r)$ must be finite and positive for every possi-

ble value of r. The function must decrease slowly, converging towards zero as r grows larger. It is essential for density functions to connect with a system that shows a finite multi-pole expansion, total mass, and effective radius. To ensure proper behavior, these descriptive functions should exhibit smooth transitions and refrain from exhibiting jump discontinuities or sudden changes. The upcoming analysis will focus on calculating the shape functions by assuming the constant as well as variable redshift function that may lead to the required WH models.

3.1 Case 1: constant redshift function

Assuming a constant redshift function is crucial in the study of traversable WHs as it simplifies the mathematical modeling of these complex structures. This assumption leads to more tractable equations that can yield analytical solutions, facilitating a better understanding of the stability and viability of WH configurations. Furthermore, a constant redshift function can help in establishing a baseline for comparison with models that incorporate variable redshifts, ultimately enhancing the robustness of theoretical predictions in any theory of gravity. Following this, we assume $\sigma(r) = c_0$ (with c_0 being a constant) that leads to its vanishing derivatives. Putting this in Eq. (13), we get

$$\rho = \frac{(\beta + 3\pi)H'(r)}{3(\beta + 2\pi)(\beta + 4\pi)r^2}. \tag{21}$$

Comparing Eqs. (19) and (21) to obtain a differential equation in terms of the EDP model provides

$$\frac{(\beta + 3\pi)H'(r)}{3(\beta + 2\pi)(\beta + 4\pi)r^2} = \rho_0 e^{-(\frac{r}{h})^{\frac{1}{n}}}, \tag{22}$$

whose solution gives

$$H(r) = c_1 - \frac{3\left(\beta^2 + 6\pi\beta + 8\pi^2\right)h^3 n\rho_0 \Gamma\left(3n, \left(\frac{r}{h^2}\right)^{\frac{1}{n}}\right)}{\beta + 3\pi}, \tag{23}$$

with c_1 being the constant that can be determined by applying the condition $H(r_0) = r_0$. Using this condition, we obtain

$$c_1 = \frac{3\left(\beta^2 + 6\pi\beta + 8\pi^2\right)h^3 n\rho_0 \Gamma\left(3n, \left(\frac{r_0}{h^2}\right)^{\frac{1}{n}}\right)}{\beta + 3\pi} + r_0. \tag{24}$$

Substituting this back into Eq. (30) results in the following expression for the shape function as

$$H(r) = \frac{3\left(\beta^2 + 6\pi\beta + 8\pi^2\right)h^3 n\rho_0 \Gamma\left(3n, \left(\frac{r_0}{h^2}\right)^{\frac{1}{n}}\right)}{\beta + 3\pi} + r_0$$
$$- \frac{3\left(\beta^2 + 6\pi\beta + 8\pi^2\right)h^3 n\rho_0 \Gamma\left(3n, \left(\frac{r}{h^2}\right)^{\frac{1}{n}}\right)}{\beta + 3\pi}. \tag{25}$$

Figure 1 verifies the condition of asymptotic flatness for the above shape function and we find the ratio of $H(r)$ to r approaches zero when r approaches infinity. The other four conditions are also plotted in the same figure from which we also observe the fulfilment of the so-called flaring-out condition. Another requirement for $H(r)$ to be fulfilled is that it must be less than r for all values of r. The upper right graph reveals the location of the WH throat at $r_0 = 0.5$, where the curve $H(r) - r$ crosses the radial axis. Finally, the resulting matter variables (13)–(15) in terms of the function (25) are

$$\rho = \frac{1}{h^3}\left[r^3\rho_0 e^{-\left(\frac{r}{h^2}\right)^{\frac{1}{n}}}\right], \tag{26}$$

$$\begin{aligned} P_r = {} & \frac{1}{2(\beta + 2\pi)(\beta + 4\pi)r^3}\left[\frac{1}{h^3(\beta + 3\pi)}\right. \\ & \times \left\{\beta(\beta + 2\pi)(\beta + 4\pi)r^3\rho_0 e^{-\left(\frac{r}{h^2}\right)^{\frac{1}{n}}}\right\} \\ & - \frac{1}{\beta + 9.42478}\left\{3(\beta + 6.28319)\right. \\ & \times \left(0.166667\beta + h^3 n\rho_0(\beta^2 + 18.8496\beta + 78.9568)\Gamma\right. \\ & \times \left(3n, \left(\frac{0.5}{h^2}\right)^{\frac{1}{n}}\right)\rho_0 - (\beta^2 + 18.8496\beta + 78.9568) \\ & \left.\left.\left.\times \Gamma\left(3n, \left(\frac{r}{h^2}\right)^{\frac{1}{n}}\right) + 1.5708h^3 n\rho_0\right)\right\}\Bigg], \end{aligned} \tag{27}$$

$$\begin{aligned} P_t = {} & -\frac{1}{4(\beta + 2\pi)(\beta + 4\pi)r^3}\left[\frac{1}{h^3(\beta + 3\pi)}\right. \\ & \times \left\{(\beta + 2\pi)(\beta + 4\pi)(\beta + 6\pi)r^3\rho_0\right. \\ & \left.\times e^{-\left(\frac{r}{h^2}\right)^{\frac{1}{n}}}\right\} - \frac{1}{\beta + 9.42478}\left\{3(\beta + 6.28319)\right. \\ & \times \left(0.166667\beta + h^3 n\rho_0\right\}\left\{(\beta^2 + 18.8496\beta + 78.9568)\Gamma\right. \\ & \times \left(3n, \left(\frac{0.5}{h^2}\right)^{\frac{1}{n}}\right) - (\beta^2 + 18.8496\beta + 78.9568) \\ & \left.\left.\left.\times \Gamma\left(3n, \left(\frac{r}{h^2}\right)^{\frac{1}{n}}\right)\right\} + 1.5708\right)\right\}\Bigg]. \end{aligned} \tag{28}$$

Energy conditions are key constraints in theoretical physics because they influence the distribution of energy and momentum within the fabric of spacetime. These conditions are crucial for fully comprehending the interactions between matter and energy. The universe is made up of several substances, such as ordinary/baryonic matter, dark and exotic fluids, and dark energy. Variations in the behavior of each category depend on the specific physical conditions under con-

sideration. Hence, determining the viable geometry proves to be a considerable challenge for researchers in this field.

Achieving a traversable WH requires violating these conditions. Exotic matter is confirmed to exist when energy constraints are violated. The recognized categories include four types: null (NECs), weak, dominant, and strong. The satisfaction of NECs has a profound impact on the other bounds in such a way that failure to meet NECs leads to the violation of all others. In conclusion, our analysis of WH solutions is entirely centered on NECs. They are given as [87–91]

$$\rho + P_r \geq 0, \quad \rho + P_t \geq 0.$$

In Fig. 2, the plots of NECs are illustrated for the solution (26)–(28) with parameters $\rho_0 = 2$, $n = 2, 3$, $\beta = 0.5, 1.5, 2.5, 3.5, 4.5$, and $h = 1$. These plots demonstrate how the conditions respond to different values of the parameters. It is found that the NECs are not satisfied, regardless of the parametric values used. This result highlights a significant conclusion that the possible theoretical model for a traversable WH contains exotic fluid. The significance of this discovery lies in its potential to impact future scientific investigations and practical uses in WH physics, setting the stage for additional exploration and validation.

3.2 Case 2: variable redshift function

Assuming a variable redshift function in the study of traversable WHs is also crucial. Unlike constant redshift functions, which imply a uniform gravitational field, variable redshift functions allow for a more nuanced understanding of how gravitational effects can change with distance. This variability can lead to different causal structures and stability conditions for the WH, influencing the feasibility of traversing these structures. Following this, we adopt the redshift function as $\sigma(r) = \frac{-2\lambda}{r}$ with λ being a free parameter. We firstly equate Eqs. (10) and (19) to calculate the shape function, however, the resulting equation becomes so complex such that it is unable to be solved analytically. So we use another approach by equating the effective energy density (13) and (19), resulting in the differential equation expressed by

$$\frac{H'(r)}{8\pi r^2} = \rho_0 e^{-(\frac{r}{h})^{\frac{1}{n}}}. \tag{29}$$

The shape function in the light of above equation has the following expression

$$H(r) = c_2 - 8\pi h^3 n\rho_0 \Gamma\left(3n, \left(\frac{r}{h}\right)^{\frac{1}{n}}\right). \tag{30}$$

The constant c_2 can be extracted by applying the condition $H(r_0) = r_0$ given by

$$c_2 = 8\pi h^3 n\rho_0 \Gamma\left(3n, \left(\frac{r_0}{h}\right)^{\frac{1}{n}}\right) + r_0, \tag{31}$$

whose substitution into Eq. (30) results in the ultimate expression for $H(r)$ as

$$H(r) = 8\pi h^3 n\rho_0 \Gamma\left(3n, \left(\frac{r_0}{h}\right)^{\frac{1}{n}}\right) - 8\pi h^3 n\rho_0 \Gamma\left(3n, \left(\frac{r}{h}\right)^{\frac{1}{n}}\right) + r_0. \tag{32}$$

The behavior of the shape function is illustrated in Fig. 3. All the conditions involving flaring-out and asymptotic flatness are observed to be fulfilled. Further, the throat is found to be the same as we already determined in the case of constant redshift, i.e., $r = 0.5$. The final expressions of fluid triplet for the shape function (32) are presented as

$$\begin{aligned}
\rho = {} & \frac{e^{-\left(\frac{r}{h}\right)^{\frac{1}{n}}}}{(\beta + 6.28319)(\beta + 12.5664)r^5} \\
& \times \Bigg[\Bigg(1.0472\beta\lambda + 8.37758r\beta + 78.9568r\Bigg) \\
& \times h^3 r^4 \rho_0 + \beta\lambda e^{\left(\frac{r}{h}\right)^{\frac{1}{n}}} \\
& \times \Bigg\{h^3 n\rho_0 \Bigg((1.0472r - 2.0944\lambda)\Gamma\left(3n, 0.5^{\frac{1}{n}}\left(\frac{1}{h}\right)^{\frac{1}{n}}\right) \\
& + (2.0944\lambda - 1.0472r)\Gamma\left(3n, \left(\frac{r}{h}\right)^{\frac{1}{n}}\right)\Bigg) \\
& - 0.0416667\lambda + (0.0833333\lambda + 0.0208333)r\Bigg\}\Bigg],
\end{aligned} \tag{33}$$

$$\begin{aligned}
P_r = {} & \frac{1}{48(\beta + 2\pi)(\beta + 4\pi)r^5} \\
& \times \Bigg[\Bigg\{16\pi\beta r^4 \rho_0 (4r - \lambda) e^{-\left(\frac{r}{h}\right)^{\frac{1}{n}}} + 48\lambda r^2(\beta + 2\pi) \\
& - 4r\beta\lambda^2\Bigg\}4r - 192\Bigg\{r^2(1.\beta + 6.28319) \\
& - 0.166667\beta\lambda^2 + \lambda r(2.08333\beta + 12.5664)\Bigg\} \\
& \times \Bigg\{0.0625 + h^3 n\rho_0 \pi \Gamma\left(3n, 0.5^{\frac{1}{n}}\left(\frac{1}{h}\right)^{\frac{1}{n}}\right) \\
& - 3.14159h^3 n\rho_0 \times \Gamma\left(3n, \left(\frac{r}{h}\right)^{\frac{1}{n}}\right)\Bigg\}\Bigg],
\end{aligned} \tag{34}$$

$$\begin{aligned}
P_t = {} & \frac{1}{48(\beta + 2\pi)(\beta + 4\pi)r^5} \\
& \times \Bigg[96\Bigg\{(\beta + 6.28319)r^2 - (1.66667\beta + 12.5664)\lambda^2 \\
& + (2.83333\beta + 18.8496)\lambda r\Bigg\} \\
& \times \Bigg\{h^3 n\rho_0 \pi \Gamma\left(3n, 0.5^{\frac{1}{n}}\left(\frac{1}{h}\right)^{\frac{1}{n}}\right) - 3.14159h^3 n\rho_0
\end{aligned}$$

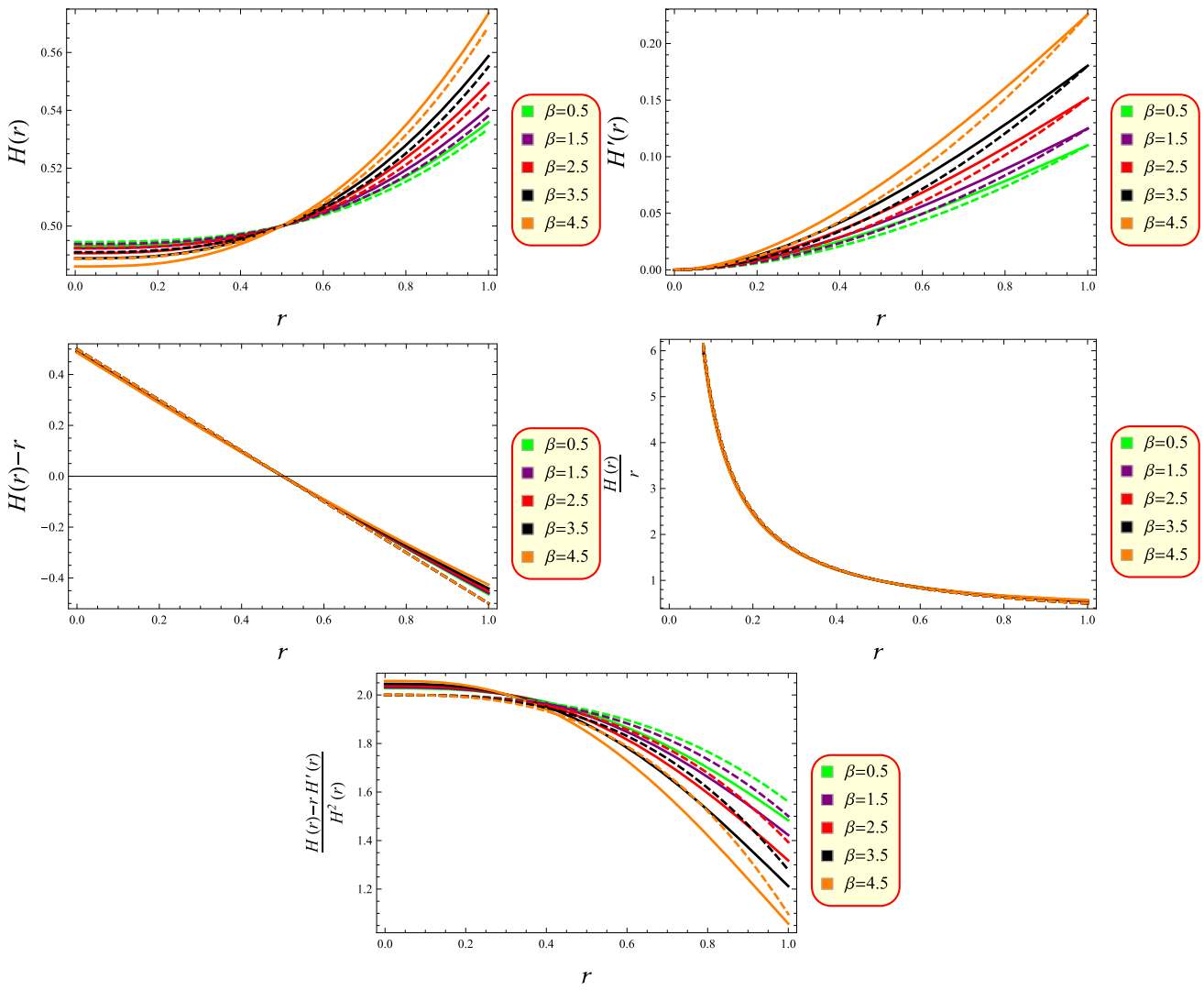

Fig. 1 Shape function (25) versus r

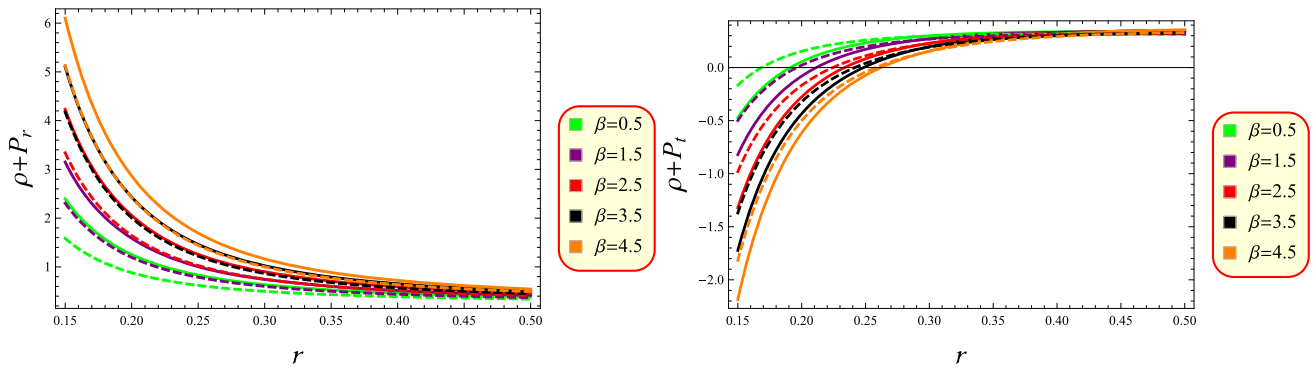

Fig. 2 NECs for case 1

$$\times \Gamma\left(3n, \left(\frac{r}{h}\right)^{\frac{1}{n}}\right) + 0.0625\Big\} + 4r\lambda\left(5\beta\lambda - 6\beta r + 12\pi(\lambda - r)\right) - 16\pi r^3\rho_0 \times e^{-\left(\frac{r}{h}\right)^{\frac{1}{n}}}\left(\beta(2r - 5\lambda) + 12\pi(r - \lambda)\right)\Big]. \tag{35}$$

The analysis of NECs is depicted in Fig. 4 by utilizing the same values of all parameters which are already used in the case of constant redshift. The plots confirm that the NECs are unsatisfied across the whole domain, irrespective of the chosen values for β and n. This non-fulfillment of the NECs implies that the chosen parameter configuration is crucial for achieving the a traversable WH model. This points to the possible limitations, indicating that achieving the desired WH models could be problematic with alternative parametric choices or when we are working in other gravity theories. This illustrates the necessity for continued investigation to modify these choices to satisfy the criteria for the existence of a traversable WH.

4 Active gravitational mass

We explore the active gravitational mass related to the dark matter WHs in this section. Active gravitational mass is defined within the context of the WH's geometry, particularly from the throat radius r_0 to the outer boundary at radius r. It is calculated using the following expression

$$M_A = 4\pi \int_{r_0}^{r} r^2\rho(r)dr, \tag{36}$$

which indicates that the mass increases as one approaches the throat. This relationship highlights the significant role of the throat in dictating the gravitational influence of the WH, as the active mass contributes to the overall gravitational field experienced in its vicinity. It must be mentioned here that the active gravitational mass and the complexity factor (which shall be discussed in the next section) are originally defined from 0 up to some value of r. However, in the case of WHs, the lower limit cannot be 0 because this point does not belong to the manifold. While discussing such hypothetical structures, this limit becomes r_0 to r with $r \in (r_0, \infty)$ to properly define both the above quantities [92]. We also note that the standard definition demands $r_0 = 0$, but this case must be discarded to ensure a finite size of the WH throat.

In the case of constant redshift function, the above mass can be calculated by using Eq.(26) as

$$M_A = \frac{4\pi}{(\beta + 2\pi)(\beta + 4\pi)}\Bigg[h^3 n\rho_0\Gamma\left(3n, \left(\frac{0.5}{h^2}\right)^{\frac{1}{n}}\right) \times\left(\beta^2 + 6\pi\beta + 8\pi^2\right) - h^3 n\rho_0\Gamma\left(3n, \left(\frac{r}{h^2}\right)^{\frac{1}{n}}\right) \times\left(\beta^2 + 6\pi\beta + 8\pi^2\right) + 0.1667(\beta + 3\pi)\Bigg]. \tag{37}$$

However, we obtain much lengthy expression of the mass function corresponding to the variable redshift and thus its value is not provided here. The behavior of M_A for a traversable WH analogous to both the cases is shown in Fig. 5 using already chosen values of Einasto index and $f(R, T)$ model parameter. We observe that the plots initially take the negative values and then increase when r grows. It is important to highlight here that the mass becomes negative near the WH throat. The occurrence of negative mass in a certain spatial area implies the existence of exotic matter and a breach of energy conditions. Such a behavior also confirms the existence of traversable WH models for both the considered redshift cases.

5 Complexity factor in wormholes

In 2018, Herrera proposed a comprehensive definition of the complexity for compact objects exhibiting a static spherical symmetry [93]. He used the Bel's idea of splitting the curvature tensor orthogonally and derived some scalars, one of them was referred to the complexity factor. The formulation of this factor was based on the systems which are simple or minimally complex, characterized by isotropic pressure and uniform energy density. A zero complexity factor characterizes this type of fluid distribution. To analyze different cosmic stellar solutions, including Bondi and axial metrics, the complexity factor has been investigated [94–100]. Additionally, the complexity factor of compact systems coupled with anisotropic pressure and inhomogeneous energy density reduces to zero only when their effects cancel each other [101–108]. For the case of modified $f(R, T)$ gravity, the complexity factor is specified in the following manner

$$Y_{TF}(r) = 8\pi\Pi(1 + \beta) - \frac{4\pi}{r^3}\int_{r_0}^{r} r^3\rho'(r)dr, \tag{38}$$

with $\Pi = P_r - P_t$ being the anisotropic pressure. When putting the values of the fluid triplet (26)–(28) for the case of constant redshift, we get the following expression

$$Y_{TF} = \frac{2\pi\beta(3\beta + 6\pi + 1)}{r^3(\beta + 2\pi)(\beta + 4\pi)}$$

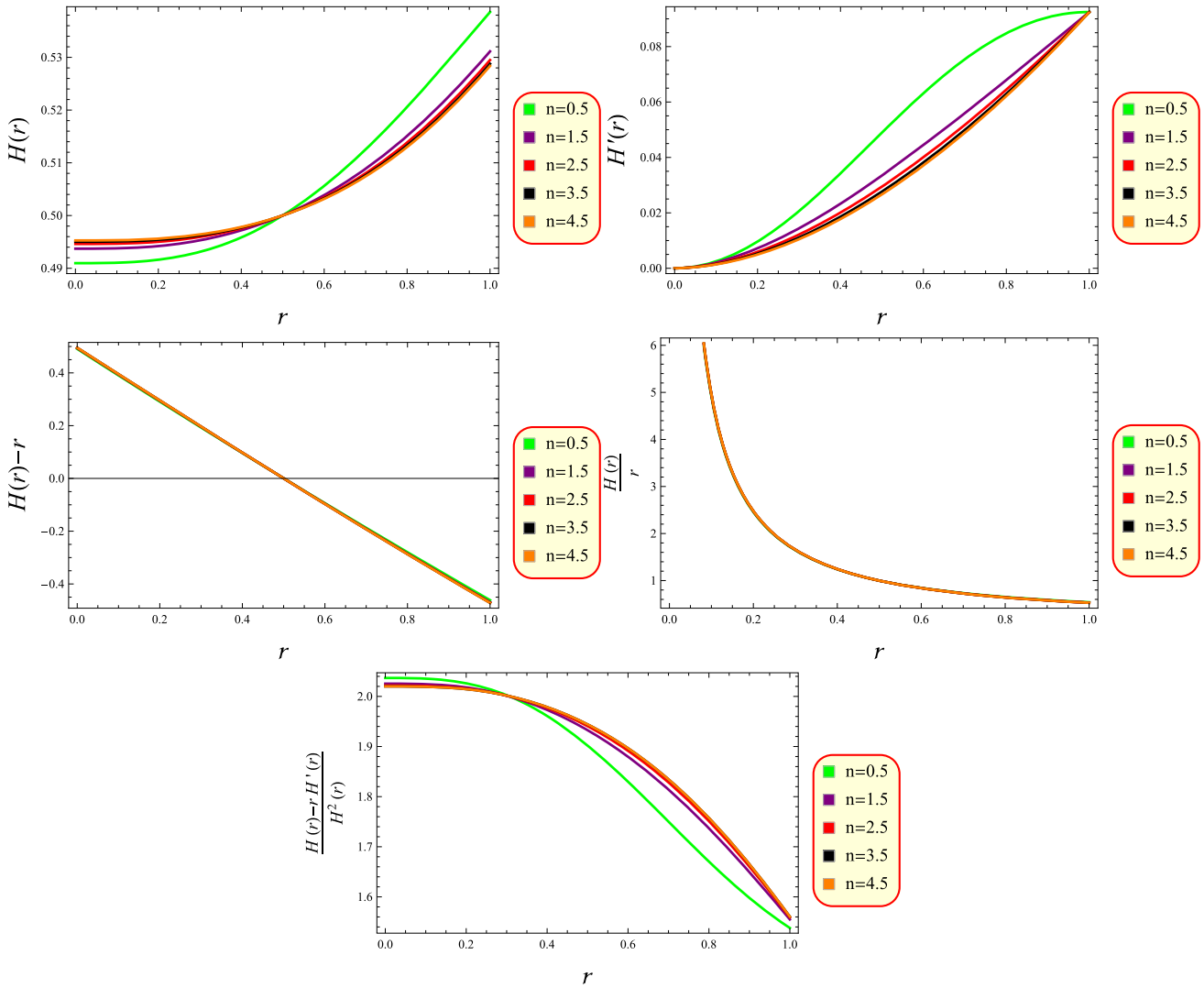

Fig. 3 Shape function (32) versus r

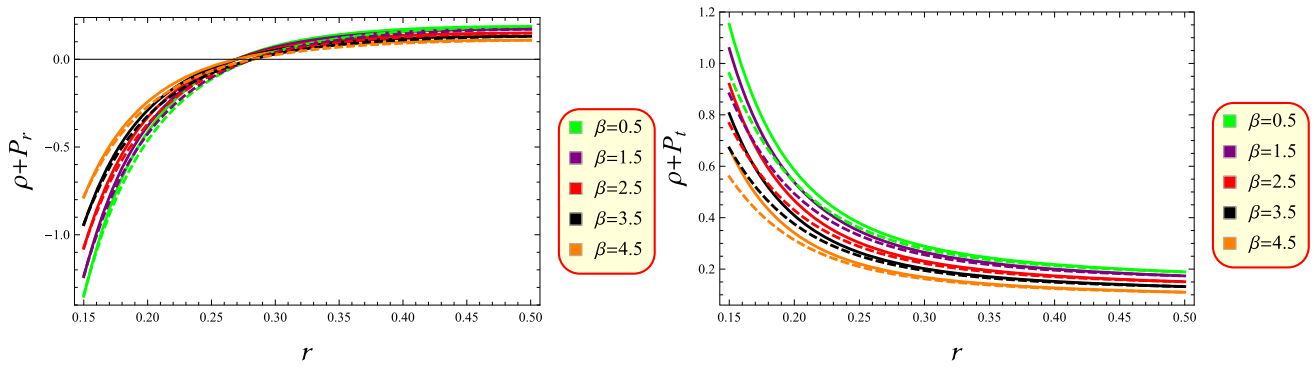

Fig. 4 NECs for case 2

$$\times\left[\left(\beta^2+6\pi\beta+8\pi^2\right)hr\rho_0 e^{-\left(\frac{r}{h^2}\right)^{\frac{1}{n}}}\left(\frac{r}{h^2}\right)^{\frac{1}{n}-1}\right.$$
$$\times\left(\frac{r}{h^2}\right)^{\frac{3n-1}{n}}+3\left(\beta^2+6\pi\beta+8\pi^2\right)h^3n\rho_0\Gamma$$
$$\times\left(3n,\left(\frac{r}{h^2}\right)^{\frac{1}{n}}\right)-3\left(\beta^2+6\pi\beta+8\pi^2\right)h^3n\rho_0$$
$$\left.\times\Gamma\left(3n,\left(\frac{0.5}{h^2}\right)^{\frac{1}{n}}\right)-0.5(\beta+3\pi)\right]. \tag{39}$$

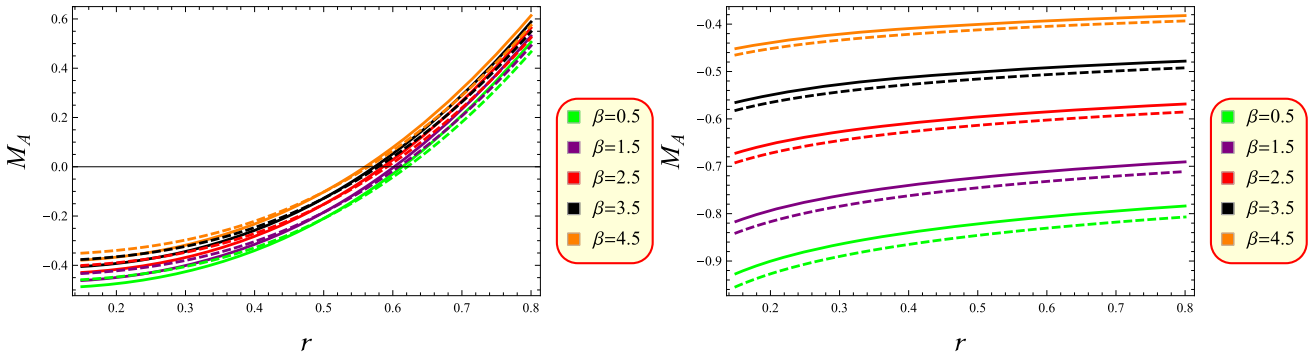

Fig. 5 Active gravitational mass for cases 1 (left) and 2 (right)

Figure 6 depicts the variation of the complexity factor with respect to the radial coordinate r for case 1. As r extends towards infinity or moves farther from the WH throat, Y_{TF} is seen to approach zero. With the increase in radial coordinates, Y_{TF} reduces towards zero, while the complexity element slowly progresses towards the WH throat and becomes maximum near this point.

On the other hand, the expression for the complexity factor corresponding to case 2 is not provided due to its lengthy expression, however, its graphical representation is shown in Fig. 6 (right plot). The graph shows that the factor Y_{TF} possesses the same behavior as found in case 1.

6 Stability evaluation

Celestial geometries are difficult to study because their persistent response to external disturbances complicates the extraction of valuable insights. The formulation of scientific models and the development of reliable hypotheses about the structure's evolution can be impeded by these disturbing factors. Evaluating the validity of celestial bodies is significantly reliant on their stability, which is fundamental in selecting which objects deserve a more detailed investigation. Here,"stability" illustrates the ability of a celestial geometry to uphold its structure over long timescales even when influenced by external disturbances.

The stability of WH structures is more often analyzed through quasinormal modes [109,110] as the study of cracking and adiabatic index is valuable for interior solutions. However, there exist some works in this context that agree with the exploration of sound speed and cracking approach in order to analyze the stability of developed WH models [111–113]. We, therefore, proceed with the later methodologies in the following subsections to check whether our constructed solutions are stable or not.

6.1 Causality and cracking

The rate at which sound or pressure waves travel through different materials is known as sound speed. This investigation focuses on the rate at which these waves propagate through the WH. The findings show how internal pressure can counteract the gravitational effects present within the WH. To avoid collapse and maintain stability, a WH requires enough pressure to counter the effects of gravity. The presence of internal disturbances might lead to instability in the WH. Under the causality condition, the speed of sound must be restricted to the interval [0, 1] [114,115]. The way in which pressure's change with respect to density is represented by the components given below

$$v_r^2 = \frac{dP_r}{d\rho}, \quad v_t^2 = \frac{dP_t}{d\rho}.$$

The pressure variations due to internal forces are measured by the radial component. Also, the other factor assesses the object's response to external pressure. Figure 7 displays the plots of these components, showing the agreeable profile.

The concept of cracking, as introduced by Herrera [116], is utilized to address inconsistencies in self-gravitating systems, such as WHs. His study suggests that stability in a self-gravitating system is maintained when the absolute difference between the sound speed components lies within the interval of 0 to 1, such that $0 \leq |v_t^2 - v_r^2| \leq 1$. The plots in Fig. 8 show physically valid WH structures for all values of β and n.

6.2 Adiabatic index

This factor, which yields crucial insights into fluid thermodynamics, is also important for assessing the stability of celestial systems such as neutron stars, WHs and others. The energy flow within a spacetime configuration is better understood through this factor. For the system to be stable, the factor Γ must be greater than $\frac{4}{3}$. If this limit is not fulfilled, the system will become unstable [117–120]. Here are the expressions for this across two distinct directions as

$$\Gamma_r = \frac{\rho + P_r}{P_r}\frac{dP_r}{d\rho}, \quad \Gamma_t = \frac{\rho + P_t}{P_t}\frac{dP_t}{d\rho}.$$

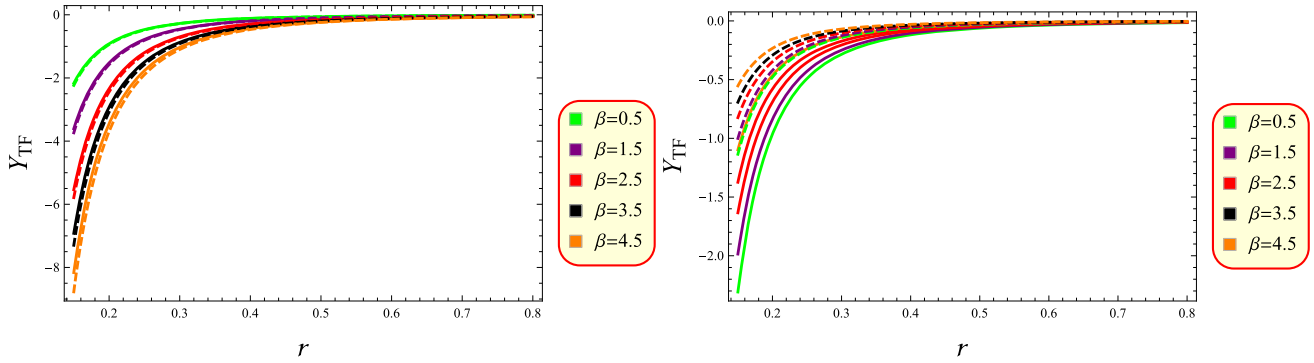

Fig. 6 Complexity factor for cases 1 (left) and 2 (right)

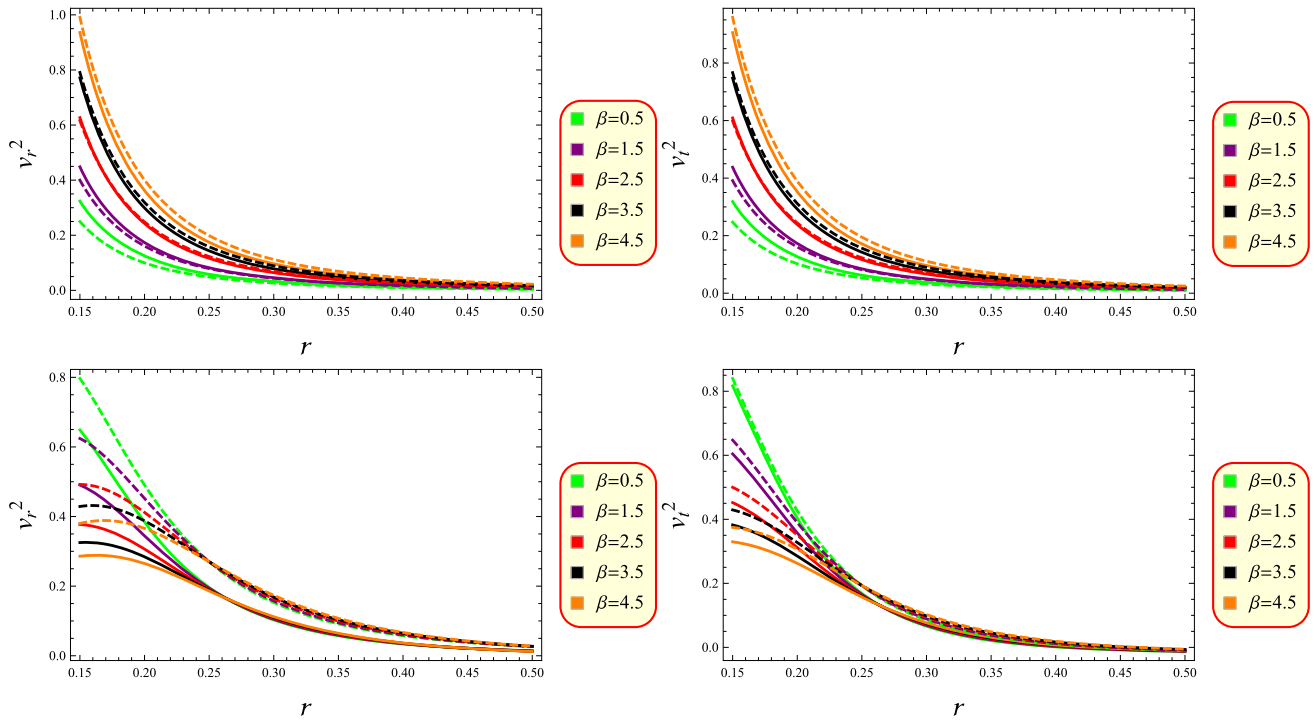

Fig. 7 Causality for cases 1 (upper) and 2 (lower)

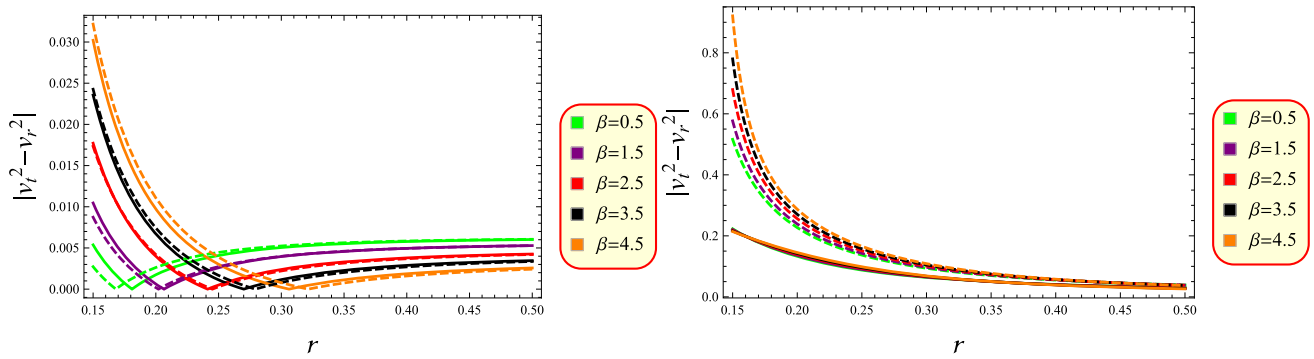

Fig. 8 Cracking for cases 1 (left) and 2 (right)

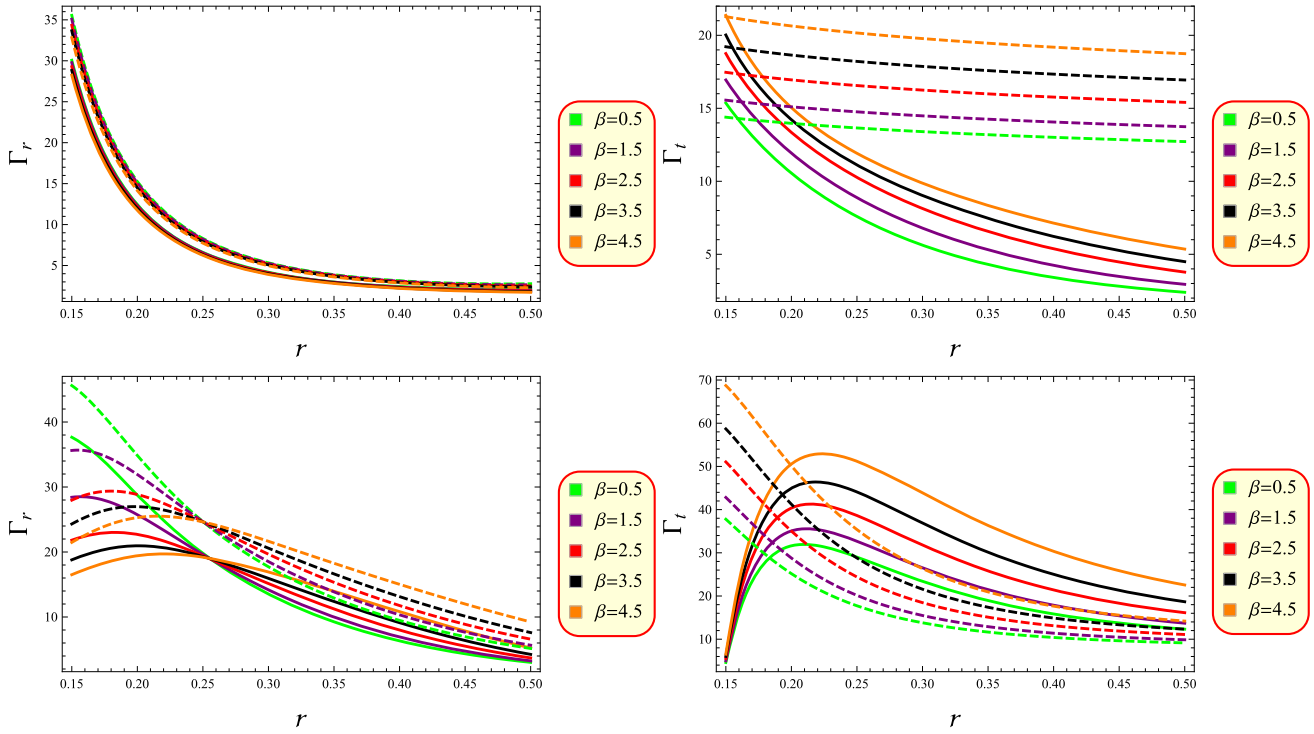

Fig. 9 Adiabatic index for cases 1 (upper) and 2 (lower)

Such a statement may not be promising as the above condition is necessary but not a sufficient one. Its main drawback is that it does not include the anisotropic factor in its explicit form, which plays a fundamental role in the stability of the fluid distribution. Indeed, according to Chandrasekhar [121], the condition for the stability of a Newtonian isotropic sphere is $\Gamma > \frac{4}{3}$ (for details, see [122]). However, this condition changes for a relativistic isotropic sphere [122], and more so for an anisotropic general relativistic (or Newtonian) sphere. A thorough discussion on the influence of the anisotropy on the stability of the fluid configuration, in terms of the adiabatic index was carried on in [123–126]. It was found that in the Newtonian limit, the unstable range of Γ is given by

$$\Gamma < \frac{4}{3} - \left[\frac{4}{3}\frac{P_{r0} - P_{t0}}{|P'_{r0}|r}\right]_{max},$$

where the subscript 0 denotes the quantity before perturbation (in equilibrium). We, therefore, conclude that the pressure anisotropy in this case may decrease or increase the range of instability, depending on the sign of the anisotropic factor. In the post-Newtonian approximation, the corresponding expression reads

$$\Gamma < \frac{4}{3} - \left[\frac{4}{3}\frac{P_{r0} - P_{t0}}{|P'_{r0}|r} - \frac{8\pi P_{r0} r}{3|P'_{r0}|}\right]_{max},$$

indicating that the anisotropic factor remains the same, and the gravitational term increases the unstable range of Γ due to the regenerative effect of the radial pressure.

As shown in Fig. 9, stable WH solutions are attained because the requisite condition is satisfied in modified $f(R, T)$ gravity. The successful formulation of the WH models in stability tests leads us to conclude that this modified theory is trustworthy for analyzing WH solutions derived from both constant and variable redshift functions.

7 Conclusions

This paper is aimed at observing the effect of EDP model on the possible existence of WH geometries within the framework of modified $f(R, T)$ theory. We have started our analysis with the introduction of modified theory and developed the corresponding anisotropic equations of motion using a minimal model. The EDP model has then been taken into account to discuss the imprints of dark matter halos on the formulating solutions. After this, we have assume two different cases of the redshift function such as constant and variable, and determined their corresponding shape functions. Both shape functions admitted the integration constants which have been calculated through the condition $H(r_0) = r_0$. The NECs have also been checked for both models by adopting different parametric values. Further, the active gravitational mass, complexity factor and stability tests have also been discussed

from which we found some interesting results. The key points of our investigation are enclosed in the following.

- The shape functions for both cases 1 and 2 meet all required conditions, including the flatness condition, which is satisfied for positive values of H (Figs. 1 and 3). The throat is found to be 0.5 in both cases. The validation of the shape functions' criteria confirm their applicability in deriving WH solutions.
- We have chosen specific parametric values as $n = 2, 3$, $h = 1$, $\rho_0 = 2$, and $\beta = 0.5, 1.5, 2.5, 3.5, 4.5$ to further analyze the NECs and find them in the negative range (Figs. 2 and 4). The consistent failure of NECs across various parametric choices suggests that exotic matter is present in the WH throat. Therefore, the identification of a traversable WH solution has been achieved successfully. Also, it is crucial to keep in mind that the existence of WH structures is contingent upon specific parameter values. Adjusting these values could lead to a major change in the observed outcomes.
- The profile of the active gravitational mass is also discussed. We find this to be negative in certain regions, in particular, near the throat of WH (Fig. 5). However, this is not entirely based on the violation of the NECs since negative densities can lead to positive masses because what matters is the area under the curve. Furthermore, a negative mass implies repulsive gravity. But in the current scenario, this negative behavior might be occurred due to two particular shape functions which are derived by using EDP that provides some key parameters to accurately describe different dark matter halos or galaxy clusters.
- Moreover, we derive the complexity factor through orthogonal splitting of the Riemann tensor in this modified theory by following the Herrera's recently proposed definition [93]. The inverse trend between radial coordinate and Y_{TF} shows that the complexity factor reaches its maximum near the WH throat and approaches zero as it moves farther from this point (Fig. 6).
- A comprehensive analysis of the model's stability is also performed. Different stability tests have been applied to the resulting two models and we conclude that each of them demonstrates stability under all the evaluated approaches (Figs. 7, 8, 9).

It is important to highlight that the developed results are found to be consistent with existing works under the assumption of a linear equation of state [16,49,50]. Furthermore, the results of this study are well-aligned with observations from other gravity theories, such as GR [127] and $f(R)$ framework [128]. We can reduce our results in GR by substituting $\beta = 0$ in the model (9).

Acknowledgements Baiju Dayanandan acknowledges support from the Authority of University of Nizwa, Nizwa, Sultanate of Oman.

Funding This research received no external funding.

Data Availability Statement My manuscript has no associated data. [Authors' comment: No additional data were analyzed or created as part of this study.]

Code Availability Statement My manuscript has no associated code/software. [Authors' comment: Code/Software sharing not applicable to this article as no code/software was generated or analysed during the current study.]

Funded by SCOAP[3].

References

1. A.G. Riess et al., Astron. J. **116**, 1009 (1998)
2. S. Perlmutter et al., Astrophys. J. **517**, 565 (1999)
3. S. Perlmutter et al., Astrophys. J. **483**, 565 (1997)
4. S. Perlmutter et al., Nature **391**, 51 (1998)
5. S. Perlmutter et al., Astrophys. J. **517**, 565 (1999)
6. H.A. Buchdahl, Mon. Not. R. Astron. Soc. **150**, 1 (1970)
7. S. Nojiri, S.D. Odintsov, Phys. Rev. D **68**, 123512 (2003)
8. Y.S. Song, W. Hu, I. Sawicki, Phys. Rev. D **75**, 044004 (2007)
9. S. Nojiri, S.D. Odintsov, Phys. Rep. **505**, 59 (2011)
10. T. Naseer, M. Sharif, Phys. Dark Univ. **46**, 101595 (2024)
11. T. Naseer, M. Sharif, Eur. Phys. J. C **84**, 554 (2024)
12. K. Bamba, S. Capozziello, S. Nojiri, S.D. Odintsov, Astrophys. Space Sci. **342**, 155 (2012)
13. S. Nojiri, S.D. Odintsov, Int. J. Geom. Methods Mod. Phys. **11**, 1460006 (2014)
14. A.S. Agrawal, S.K. Tripathy, B. Mishra, Chin. J. Phys. **71**, 333 (2021)
15. O. Bertolami, C.G. Boehmer, T. Harko, F.S.N. Lobo, Phys. Rev. D **75**, 104016 (2007)
16. T. Naseer, M. Sharif, A. Fatima, S. Manzoor, Chin. J. Phys. **86**, 350 (2023)
17. T. Harko, F.S.N. Lobo, S. Nojiri, S.D. Odintsov, Phys. Rev. D **84**, 024020 (2011)
18. X.M. Deng, Y. Xie, Int. J. Theor. Phys. **54**, 1739 (2015)
19. C.P. Singh, P. Kumar, Eur. Phys. J. C **74**, 1 (2014)
20. M. Sharif, M. Zubair, Gen. Relativ. Gravit. **46**, 1723 (2014)
21. E.H. Baffou et al., Astrophys. Space Sci. **356**, 173 (2015)
22. P.V. Tretyakov, Eur. Phys. J. C **78**, 896 (2018)
23. S.K. Maurya, A. Errehymy, D. Deb, F. Tello-Ortiz, M. Daoud, Phys. Rev. D **100**, 044014 (2019)
24. S.K. Maurya, A. Errehymy, K. Newton Singh, F. Tello-Ortiz, M. Daoud, Phys. Dark Univ. **30**, 100640 (2020)
25. P. Rudra, K. Giri, Nucl. Phys. B **967**, 115428 (2021)

26. G.A. Carvalho, F. Rocha, H.O. Oliveira, R.V. Lobato, Eur. Phys. J. C **81**, 134 (2021)
27. J.M.Z. Pretel, S.E. Jorás, R.R.R. Reis, J.D.V. Arbañil, J. Cosmol. Astropart. Phys. **04**, 064 (2021)
28. C.Y. Chen, Y. Reyimuaji, X. Zhang, Phys. Dark Univ. **28**, 101130 (2022)
29. M. Zubair, Q. Muneer, S. Waheed, Int. J. Mod. Phys. D **31**, 2250092 (2022)
30. Y. Feng et al., Phys. Scr. **99**, 085034 (2024)
31. T. Naseer, M. Sahrif, Fortschr. Phys. **71**, 2300004 (2023)
32. M. Sharif, T. Naseer, Class. Quantum Gravity **40**, 035009 (2023)
33. T. Naseer, M. Sharif, Phys. Scr. **99**, 035001 (2024)
34. T. Naseer, M. Sharif, Commun. Theor. Phys. **76**, 095407 (2024)
35. T. Naseer, M. Sharif, Phys. Scr. **99**, 075012 (2024)
36. C.W. Misner, J.A. Wheeler, Ann. Phys. **2**, 525 (1957)
37. C.W. Misner, Phys. Rev. **118**, 1110 (1960)
38. J.A. Wheeler, Ann. Phys. **2**, 604 (1957)
39. J.A. Wheeler, Int. J. Mod. Phys. A **3**, 2207 (1988)
40. A. Einstein, N. Rosen, Phys. Rev. **48**, 73 (1935)
41. J.A. Wheeler, Phys. Rev. **97**, 511 (1955)
42. M. Sharif, T. Naseer, Indian J. Phys. **97**, 2853 (2023)
43. M. Sharif, T. Naseer, Chin. J. Phys. **85**, 41 (2023)
44. R.W. Fuller, J.A. Wheeler, Phys. Rev. **128**, 919 (1962)
45. M.S. Morris, L.S. Thorne, Am. J. Phys. **56**, 395 (1988)
46. M. Visser, Phys. Rev. D **39**, 3182 (1989)
47. S. Sushkov, Phys. Rev. D **71**, 043520 (2005)
48. F.S.N. Lobo, Phys. Rev. D **71**, 084011 (2005)
49. N.S. Kavya, V. Venkatesha, G. Mustafa, P.K. Sahoo, S.V.D. Rashmi, Chin. J. Phys. **84**, 1 (2023)
50. R. Solanki, Z. Hassan, P.K. Sahoo, Chin. J. Phys. **85**, 74 (2023)
51. E. Contreras, P. Bargueño, Int. J. Mod. Phys. D **27**, 1850101 (2018)
52. F. Tello-Ortiz, E. Contreras, Ann. Phys. **419**, 168217 (2020)
53. Z. Hassan, G. Mustafa, P.K. Sahoo, Symmetry **13**, 1260 (2021)
54. O. Sokoliuk, Z. Hassan, P.K. Sahoo, A. Baransky, Ann. Phys. **443**, 168968 (2022)
55. Z. Hassan, S. Ghosh, P.K. Sahoo, K. Bamba, Eur. Phys. J. C **82**, 1116 (2022)
56. A. Errehymy, S. Hansraj, S.K. Maurya, C. Hansraj, M. Daoud, Phys. Dark Univ. **41**, 1012 (2023)
57. A. Errehymy et al., Ann. Phys. **535**, 2300178 (2023)
58. A. Rueda, E. Contreras, Ann. Phys. **459**, 169540 (2023)
59. A. Errehymy, Phys. Dark Univ. **44**, 101438 (2024)
60. A. Errehymy et al., Chin. J. Phys. **89**, 56–68 (2024)
61. J. Einasto, Astron. Nachr. **291**, 97 (1969)
62. J. Einasto, Astrofizika **5**, 137 (1969)
63. J. Einasto, *Proceedings of the First European Astronomical Meeting Athens; Stars and the Milky Way System*, vol. 2, p. 291 (1972)
64. P.D. Alvarez et al., J. Cosmol. Astropart. Phys. **2021**, 019 (2021)
65. J.S. Peracaula, Europhys. Lett. **134**, 19001 (2021)
66. C. Moreno-Pulido, J.S. Peracaula, Eur. Phys. J. C **82**, 551 (2022)
67. J.S. Peracaula et al., Universe **9**, 262 (2023)
68. J.C. Pérez, J.S. Peracaula, Phys. Dark Univ. **43**, 101406 (2024)
69. T. Harko et al., Phys. Rev. D **84**, 024020 (2011)
70. G.A. Carvalho et al., Eur. Phys. J. C **77**, 871 (2017)
71. T.M. Ordines, E.D. Carlson, Phys. Rev. D **99**, 104052 (2019)
72. M.J.S. Houndjo, O.F. Piattella, Int. J. Mod. Phys. D **21**, 1250024 (2012)
73. M.F. Shamir, Eur. Phys. J. C **75**, 354 (2015)
74. M. Sharif, T. Naseer, Ann. Phys. **459**, 169527 (2023)
75. T. Naseer, M. Sharif, Fortschr. Phys. **72**, 2300254 (2024)
76. M. Sharif, T. Naseer, Phys. Scr. **98**, 115012 (2023)
77. M. Sharif, T. Naseer, Eur. Phys. J. Plus **139**, 86 (2024)
78. D. Merritt, A.W. Graham, B. Moore, J. Diemand, B. Terzić, Astron. J. **132**, 2685 (2006)
79. E. Hayashi, S.D. White, Mon. Not. R. Astron. Soc. **388**, 2 (2008)
80. L. Gao et al., Mon. Not. R. Astron. Soc. **387**, 536 (2008)
81. Z. Yousaf, A. Adeel, S. Khan, M.Z. Bhatti, Chin. J. Phys. **88**, 406 (2023)
82. J.F. Navarro et al., Mon. Not. R. Astron. Soc. **402**, 21 (2010)
83. P.F. de Salas, K. Malhan, K. Freese, K. Hattori, M. Valluri, J. Cosmol. Astropart. Phys. **2019**, 37 (2019)
84. D.A. Gadotti, Mon. Not. R. Astron. Soc. **393**, 1531 (2009)
85. E. Retana-Montenegro et al., Astron. Astrophys. **540**, A70 (2012)
86. J. Einasto, Astron. Nachr. **291**, 97 (1969)
87. M. Sharif, T. Naseer, Phys. Scr. **98**, 105009 (2023)
88. E. Demir et al., Chin. J. Phys. **91**, 299–315 (2024)
89. M. Sharif, T. Naseer, Pramana **98**, 25 (2024)
90. Y. Feng et al., Chin. J. Phys. **90**, 372–386 (2024)
91. T. Naseer, Phys. Dark Univ. **46**, 101663 (2024)
92. R. Avalos, E. Fuenmayor, E. Contreras, Eur. Phys. J. C **82**, 420 (2022)
93. L. Herrera, Phys. Rev. D. **97**, 044010 (2018)
94. L. Herrera, A. Di Prisco, J. Carot, Phys. Rev. D **99**, 124028 (2019)
95. Z. Yousaf, M.Z. Bhatti, T. Naseer, Phys. Dark Univ. **28**, 100535 (2020)
96. L. Herrera, Phys. Rev. D **101**, 104024 (2020)
97. Z. Yousaf, M.Z. Bhatti, T. Naseer, Eur. Phys. J. Plus **135**, 323 (2020)
98. E. Contreras, E. Fuenmayor, G. Abellán, Eur. Phys. J. C **82**, 187 (2022)
99. L. Herrera, A. Di Prisco, Phys. Rev. D **109**, 064071 (2024)
100. L. Herrera, A. Di Prisco, J. Ospino, Phys. Rev. D **109**, 024005 (2024)
101. Z. Yousaf et al., Mon. Not. R. Astron. Soc. **495**, 4334–4346 (2020)
102. Z. Yousaf, M.Z. Bhatti, T. Naseer, Int. J. Mod. Phys. D **29**, 2050061 (2020)
103. Z. Yousaf et al., Phys. Dark Univ. **29**, 100581 (2020)
104. Z. Yousaf, M.Z. Bhatti, T. Naseer, Ann. Phys. **420**, 168267 (2020)
105. S.K. Maurya, M. Govender, G. Mustafa, R. Nag, Eur. Phys. J. C **82**, 1006 (2022)
106. J. Andrade, Eur. Phys. J. C **82**, 266 (2022)
107. P. León, C.L. Heras, Eur. Phys. J. C **83**, 260 (2023)
108. J. Andrade, D. Santana, Eur. Phys. J. C **83**, 523 (2023)
109. A. Rueda, R. Avalos, E. Contreras, Eur. Phys. J. C **82**, 605 (2022)
110. R. Avalos, E. Contreras, Ann. Phys. **446**, 169128 (2022)
111. M. Sharif, A. Fatima, Eur. Phys. J. Plus **138**, 196 (2023)
112. M. Sharif, A. Fatima, Eur. Phys. J. Plus **138**, 721 (2023)
113. T. Naseer, M. Sharif, M. Faiza, Int. J. Geom. Methods Mod. Phys. 2440043 (2024)
114. H. Abreu, H. Hernández, L.A. Núnez, Class. Quantum Gravity **24**, 4631 (2007)
115. T. Naseer, J.L. Said, Eur. Phys. J. C **84**, 808 (2024)
116. L. Herrera, Phys. Lett. A **165**, 206 (1992)
117. H. Heintzmann, W. Hillebrandt, Astron. Astrophys. **38**, 51 (1975)
118. M. Sharif, T. Naseer, Eur. Phys. J. Plus **139**, 296 (2024)
119. T. Naseer, M. Sharif, Phys. Scr. **99**, 095028 (2024)
120. K. Hassan, T. Naseer, M. Sharif, Chin. J. Phys. **91**, 916 (2024)
121. S. Chandrasekhar, Mon. Not. R. Astron. Soc. **140**, 417 (1964)
122. H. Bondi, Proc. R. Soc. Lond. **A281**, 39 (1964)
123. R. Chan, S. Kichenassamy, G. Le Denmat, N.O. Santos, Mon. Not. R. Astron. Soc. **239**, 91 (1989)
124. R. Chan, L. Herrera, N.O. Santos, Mon. Not. R. Astron. Soc. **265**, 533 (1993)
125. R. Chan, L. Herrera, N.O. Santos, Class. Quantum Gravity **9**, L133 (1992)
126. R. Chan, L. Herrera, N.O. Santos, Mon. Not. R. Astron. Soc. **267**, 637 (1994)
127. I. Fayyaz, M.F. Shamir, Chin. J. Phys. **66**, 553 (2020)
128. M.F. Shamir, I. Fayyaz, Eur. Phys. J. C **80**, 1102 (2020)